J. Meas. Sci. Instrum., 2024, 15(4): 417-431. http://jmsi.publish.founderss.cn/
DOI: 10.62756/jmsi.1674-8042.2024043 jmsi@nuc.edu.cn

Acoustic location echo signal extraction of buried non-metallic pipelines based on EMD and wavelet threshold joint denoising

GE Liang[1*], YUAN Xuefeng[1], XIAO Xiaoting[2], LUO Ping[3], WANG Tian[1]

1. School of Mechanical and Electrical Engineering, Southwest Petroleum University, Chengdu 610500, China;
2. School of Electrical Engineering and Information, Southwest Petroleum University, Chengdu 610500, China;
3. China Mobile Chengdu Institute of Research and Development, Chengdu 610200, China

***Corresponding author:** GE Liang (cgroad@swpu.edu.cn)

Received: July 5, 2024 **Revised:** September 13, 2024 **Accepted:** October 15, 2024

Abstract: In the acoustic detection process of buried non-metallic pipelines, the echo signal is often interfered by a large amount of noise, which makes it extremely difficult to effectively extract useful signals. An denoising algorithm based on empirical mode decomposition (EMD) and wavelet thresholding was proposed. This method fully considered the nonlinear and non-stationary characteristics of the echo signal, making the denoising effect more significant. Its feasibility and effectiveness were verified through numerical simulation. When the input SNR (SNR_{in}) is between −10 dB and 10 dB, the output SNR (SNR_{out}) of the combined denoising algorithm increases by 12.0%—34.1% compared to the wavelet thresholding method and by 19.60%—56.8% compared to the EMD denoising method. Additionally, the RMSE of the combined denoising algorithm decreases by 18.1%—48.0% compared to the wavelet thresholding method and by 22.1%—48.8% compared to the EMD denoising method. These results indicated that this joint denoising algorithm could not only effectively reduce noise interference, but also significantly improve the positioning accuracy of acoustic detection. The research results could provide technical support for denoising the echo signals of buried non-metallic pipelines, which was conducive to improving the acoustic detection and positioning accuracy of underground non-metallic pipelines.

Key words: buried non-metallic pipeline; acoustic positioning; signal processing; optimal decomposition scale; wavelet basis function; EMD combined wavelet threshold algorithm

0 Introduction

Non-metallic pipelines are critical infrastructures for maintaining modern civilized life and carrying the nerve and lifeline of the regular operation of cities[1,2]. With the acceleration of urbanization, urban underground pipelines have become increasingly complex. During construction, the lack of complete pipeline information has led to frequent accidents, such as perforation and fracture, in daily pipeline maintenance, urban expansion, and renovation projects. Pipeline damage and fracture accidents frequently occur, resulting in significant hazards such as gas explosions, water, power outages, and heating interruptions[3-7]. To solve these problems, higher-buried pipeline detection technology and instruments are needed. An efficient and accurate pipeline detection method can provide reliable data for the distribution survey of existing underground pipelines, helping to complete the basic information of pipelines. On the other hand, it is possible to determine the location of pipelines on the construction site before construction to reduce or even eliminate damage to pipelines caused by improper construction. Among the existing non-metallic pipeline positioning methods, the acoustic pipeline positioning method has advantages such as no requirements for pipeline materials, no limitations from ground conditions, and low detection costs. It has broad market space in the future.

There are two methods for acoustic pipeline positioning technology[8]: the pipeline excitation method and the elastic wave reflection method. The pipeline excitation method injects sound waves into the pipeline[9,10] and locates the pipeline by detecting the sound waves propagating from the pipeline to the ground. However, it is necessary to have a pipe connection that can be used to inject sound waves, and the detection distance is limited. Only the horizontal position and direction of the pipe can be determined[11].

The elastic wave method uses artificial seismic sources to excite acoustic signals on the ground[12]. The amplitude of sound waves in a medium decays with increasing propagation distance, and this propagated waveform can reflect the geometric and boundary changes of the medium. However, the on-site environment of pipeline detection is complex, and numerous noises seriously affect the accuracy of pipeline acoustic detection echo signals, making it difficult to accurately obtain pipeline position information in the next step of signal analysis. How to filter out a large amount of noise in the echo signal collected by the instrument is an essential step in the pipeline positioning process, which has important practical significance for improving the accuracy and reliability of pipeline detection. The acoustic pipeline positioning method based on the elastic wave method usually uses a seismic source to excite and generate sound waves, and uses a detector array to receive echo signals. Then the received echo signals are analyzed and processed to determine the position of the pipeline[13]. However, due to factors such as the detection system and the external environment, the echo signal measured by the detector often contains noise. It may sometimes mask the original echo signal, making it challenging to obtain pipeline position information accurately in subsequent signal analysis. Therefore, pre-processing of detector data before application, such as noise reduction of detector data, is crucial.

In recent years, scholars have extensively explored and researched the acoustic detection of echo signals. In acoustic positioning, the noise components of the echo signal mainly come from environmental noise, equipment noise, and reflection and scattering noise. Environmental noise, including natural sounds such as wind and rain, and human factors such as traffic noise, can interfere with sound signals, especially in urban environments. The equipment noise mainly refers to the self-noise generated by sensors and signal processing equipment during operation. When sound waves encounter interfaces with different materials, such as soil and rocks, some will be reflected and scattered, forming reflection and scattering noise.

To reduce the impact of these noises on the quality of echo signals, roughly three types of echo signal denoising methods are widely used. The first type is the estimation filtering method. This type is achieved by estimating the correlation of the echo signal and then using these calculated values to design filters for signal-filtering processing. This method is proposed on the basis of linearization, and is only suitable for static and linear time series analysis[14]. The second type is the wavelet threshold filtering method. This type of method centers around wavelet transform[15], which is a time-frequency multiscale analysis method with good performance in processing sharp pulse signals or signals with discontinuity[16]. The third type is the adaptive time-frequency analysis method. This type of method is based on empirical mode decomposition (EMD), which decomposes noisy signals into several IMFs, each reflecting the characteristics of the signal at different scales. The IMF components with more noisy features are removed to achieve signal denoising[17,18].

Due to the non-linear and non-stationary characteristics of the detected echo signals, the first type of method obviously cannot meet the practical needs of acoustic echo signal denoising. However, the reflected waves measured for non-metallic pipeline positioning are relatively weak, and the signal-to-noise ratio is meager. Therefore, only using wavelet threshold method or EMD method to reduce the noise of pipeline reflected wave signal is often not ideal. The wavelet threshold filtering method has poor adaptability in the signal-denoising process. After decomposing the observed signal, the EMD denoising algorithm obtains the first few low-order IMF components which are dominated by noise but mixed with some functional high-frequency signal components. Removing the high-frequency noise dominant mode inevitably leads to losing some useful signals[19,20], resulting in inaccurate subsequent pipeline positioning results. Although various denoising techniques have been used for acoustic detection echo signals, including statistical methods, wavelet transform, and wavelet threshold filtering, these methods still have limitations when dealing with signals with complex noise characteristics. For example, wavelet thresholding may result in the loss of valuable signals during denoising, while EMD methods may not effectively handle high-frequency noise[21].

A new denoising algorithm was proposed that combined empirical mode decomposition (EMD) and wavelet thresholding to provide better signal denoising performance. The acoustic positioning echo signal of buried non-metallic pipelines belongs to nonlinear non-stationary signals, which contains noise with high frequency and uneven distribution of noise intensity. It is suitable for joint denoising processing using wavelet thresholding and EMD. The method has been applied in the denoising of gear vibration signals[22], accelerometer calibration denoising[23], LiDAR signals[24], electrical imaging logging signals[25], underwater acoustic

signals[26], magnetite sorting signals[27], and steel cord conveyor belt damage signals[28]. However, the method has not yet been applied to denoising non-metallic pipeline detection echo signals.

The innovation of the proposed method lies in the special requirements for acoustic detection of underground non-metallic pipelines. It combined the advantages of EMD and wavelet denoising algorithms, and improved and optimized them to adapt to the signal characteristics of this specific application scenario. Adjusting the screening threshold (SD) in the EMD decomposition process could help this algorithm accurately identify and retain the effective components in the signal while removing noise. This optimization improved the adaptability of the algorithm to signals, especially when dealing with acoustic echo signals with nonlinear and non-stationary characteristics. This article innovatively introduced autocorrelation functions to identify the critical points of noise and valuable signal components in signals, which helped to accurately determine the modal IMF components that required wavelet thresholding after EMD decomposition. Compared with existing work, the joint denoising algorithm proposed in this study had significant improvements in signal-to-noise ratio (SNR) improvement and root mean square error (RMSE) reduction, which was of great significance for improving the accuracy of underground non-metallic pipeline detection and positioning. To further verify the effectiveness of the proposed algorithm, an experimental testing platform was built. It was not only used to test and demonstrate the performance of the algorithm in actual acoustic detection, but also proved through the analysis of actual data that the algorithm could significantly improve the SNR ratio of signals, reduce errors, and provide strong support for accurate positioning of pipeline positions.

1 Acoustic detection principle and denoising algorithm model

1.1 Principle of acoustic detection for buried non-metallic pipelines

When detecting buried non-metallic pipelines, it is necessary to determine the approximate direction of the pipeline based on the known construction data, then multiple measurement lines perpendicular to the direction of the underground pipeline are placed on the surface. The specific layout is shown in Fig.1. A seismic source is placed in the middle of each measurement line, and equally spaced detector arrays are symmetrically placed on both sides of the seismic source. When conducting field exploration, the seismic source can be located in the middle of any two adjacent detectors on the measuring line, so multiple tests can be performed on the same measuring line, which improves the accuracy of pipeline positioning. In addition, the number and spacing of detectors can be determined based on the buried depth of the tested pipeline and on-site conditions. For each measuring line in Fig.1, six detectors are used as an example. In general, the length of the measuring line should not be less than the estimated burial depth of the pipeline.

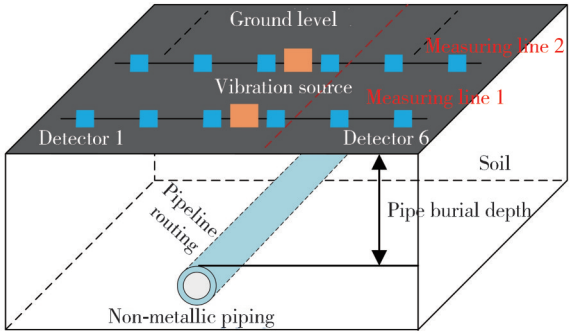

Fig. 1 Layout diagram of non-metallic pipeline positioning measurement line

Measurement line 1 is used as an example to illustrate the specific working principle. After injecting excitation signals into the seismic source, sound waves begin to radiate into the soil. The sound waves propagate through the soil and reach the surface of non-metallic pipelines after a while. Due to the differences in physical properties between the soil and the pipeline, some of the sound signals are reflected off the surface of the pipeline and transmitted upwards for a while before returning to the ground and being captured by the detector. Due to the different positions of each detector on the measuring line relative to the pipeline, the propagation distance of sound waves from the source to the soil is different from the propagation distance from the non-metallic pipeline interface to the ground, so the time for reflected echoes to reach each detector is also different. The time delay information of the detector output signal reflects the specific position information of the non-metallic pipeline relative to each detector (including the horizontal position and burial depth of the pipeline). By processing the detector signal through specific methods, the position of the non-metallic pipeline below the measurement line can be determined. It is also possible to decide on the position of non-metallic pipelines based on the measurement signals of detectors on other

measuring lines and then connect the pipeline positions obtained from each measuring line to determine the approximate direction of pipeline extension.

The optimal source excitation is a pulse signal using the time-domain superposition principle[29,30] to locate buried non-metallic pipelines[31]. At the same time, in seismic exploration, Rayleigh waves with small sidelobes and strong resolution are widely used as excitation signals for controllable seismic sources[32,33]. Therefore, Rayleigh waves are also used as the seismic source signal, that is

$$f(t)=(1-2(\pi f(t-t_0))^2)\mathrm{e}^{-(\pi f(t-t_0))^2}, \tag{1}$$

where f is the main frequency of the signal, and $t_0=\dfrac{1}{f}$ is the delay time.

1.2 EMD combined with wavelet threshold denoising algorithm model

1.2.1 Analysis of noise characteristics in echo signals

In addition to receiving various acoustic signals, the buried non-metallic pipeline detection detector can also pick up a large amount of random noise interference from both the internal instruments and the external environment. Most of these noises exhibit non-linear and non-stationary characteristics. Therefore, the measured signal of the actual detector should also include a noise component. The actual measurement signal of the detector is

$$y(t)=s(t)+n(t), \tag{2}$$

where y is the detector signal with noise pollution, and n is the noise.

The noise characteristics in the echo signal of buried non-metal pipeline are as follows. 1) Randomness. Noise usually exhibits randomness without apparent regularity and comes from various environmental factors or equipment interference. 2) High-frequency components. Noise contains many high-frequency components, which are similar in frequency to pipeline signals, leading to interference and misjudgment. 3) Nonlinear, non-stationary, and uneven intensity. The intensity of noise is unevenly distributed at different frequencies and periods, resulting in sudden high-intensity noise.

Noise is a random process, and probability density functions characterize its statistical characteristics. The noise distribution in pipeline acoustic detection can be considered Gaussian white noise following a (0, 1) distribution. The probability density function of its random variable is

$$p(x)=\frac{1}{\sqrt{2\pi\sigma}\,\mathrm{e}^{-(x-u)^2/2\sigma^2}}, \tag{3}$$

where x represents the signal amplitude; u represents the expectation of x; σ represents the standard deviation of x; and the distribution's variance is σ^2.

1.2.2 Joint algorithm model

1) Denoising principle of joint algorithm

After decomposing the original echo signal using EMD and reconstructing the low-frequency IMF components, denoising can be achieved by discarding the high-frequency components of the IMF. However, discarding specific high-frequency components may result in losing valid signal components within those high-frequency IMF. In order to retain the effective signal components in the high-frequency IMF, the proposed method calculates the auto-correlation function of the n-order IMF components after decomposing multiple IMF components through EMD. The critical point m separating noise from useful signal components is determined by analyzing the differences in autocorrelation functions between noise and signal. The high-frequency IMF components with higher noise distribution above the critical point are subjected to wavelet threshold denoising to separate useful information from noise in the high-frequency IMF components before being reconstructed with the low-frequency IMF components below the crucial point. This approach allows for the maximization of useful signal information retention while effectively reducing noise.

2) Steps of joint denoising algorithm

The specific description of the steps of the proposed joint algorithm are as follows.

(1) Identify all the local maxima and minima points on the original signal $x(t)$. Cubic spline interpolation is applied to fit the upper envelope $x_{\max}(t)$ of the signal $x(t)$ to all local maxima points, and the lower envelope $x_{\min}(t)$ is fit to all local minima points using the same method. All the data on the signal are then distributed within the range of these two envelopes.

(2) Calculate all the mean points of the upper and lower envelopes and connect them to obtain the mean envelope $m_1(t)$ as

$$m_1(t)=\frac{x_{\max}(t)+x_{\min}(t)}{2}. \tag{4}$$

Next, the mean envelope $m_1(t)$ is subtracted from the original signal $x(t)$ to obtain $h_1(t)$ as

$$h_1(t)=x(t)-m_1(t). \tag{5}$$

If $h_1(t)$ meets the requirements a and b defined for an IMF, then the first-order IMF component of the original

signal is obtained.

(3) If it does not meet the requirements, $h_1(t)$ is considered as the original signal, and steps (1) and (2) are repeated to obtain a new mean $m_{11}(t)$, and then $h_{11}(t)=h_1(t)-m_{11}(t)$. The adequacy of $h_{11}(t)$ to requirements a and b is assessed again. If it does not meet the criteria, the process is repeated. And after k repetitions, there is

$$h_{1k}(t)=h_{1(k-1)}(t)-m_{1k}(t). \tag{6}$$

Whether the data $h_{1k}(t)$ selected in the kth iteration meets the requirements of an IMF component can be determined by comparing it against the sifting threshold defined in the mathematical expression, that is

$$SD=\sum_{t=0}^{T}\left|\frac{|h_{1(k-1)}(t)-h_{1k}(t)|^2}{h_{1(k-1)}^2(t)}\right|. \tag{7}$$

It is assumed that the number of filtering iterations is too many, although the IMF component is increased, the stability and linearity are improved. In that case, the IMF components obtained may become a frequency-modulated wave with constant amplitude, thereby failing to describe the amplitude variations of the signal accurately. On the other hand, if the number of iterations is too low, the obtained components may not meet the requirements for IMF components. Therefore, the value of SD needs to be carefully selected. Research suggests that $0.2<SD<0.3$ is a more suitable choice.

When $h_{1k}(t)$ meets the conditions of SD, the sifting process stops. The obtained $h_{1k}(t)$ is retained as the first-order IMF component of the signal $x(t)$ and denoted as

$$c_1(t)=h_{1k}(t), \tag{8}$$

where $r_1(t)$ represents the residual component after removing the high-frequency component.

(4) Removing $c_1(t)$ from $x(t)$, it can be obtained that

$$r_1(t)=x(t)-c_1(t). \tag{9}$$

Taking $r_1(t)$ as a new set of original signals, the second order IMF component $c_2(t)$ of signal $x(t)$ is obtained by continuous screening operations (1) — (3). By continuing the decomposition steps mentioned above, after n iterations, the nth-order IMF component can be obtained, at which point the residual (also known as the trend term) is

$$r_n(t)=r_{n-1}(t)-c_n(t). \tag{10}$$

In the mathematical expression above, each IMF component $c_1(t)$ to $c_n(t)$ contains information from different frequency bands of the original signal, with the frequency bands changing sequentially from high to low.

If $c_n(t)$ is within a given error range, or $r_n(t)$ becomes a monotone or constant function, then the mode decomposition process terminates. In this case, the original signal can be expressed as the sum of n IMF components and residials.

$$x(t)=\sum_{i=1}^{n}c_i(t)+r_n(t). \tag{11}$$

(5) The formula for calculating the autocorrelation function of the nth IMF component is

$$R_i=E[c_i(t)c_i(t+\tau)]. \tag{12}$$

According to the difference between the characteristics of noise and signal autocorrelation function, the critical point m of noise and valuable signal component is determined[34].

(6) Select appropriate wavelet basis functions and decomposition levels.

(7) Select the threshold function. After the threshold value is obtained, the soft threshold function is selected for denoising to keep the waveform smooth and minimize the information loss and signal distortion. The original wavelet coefficient obtained after wavelet decomposition is represented by w, and the wavelet coefficient is obtained after threshold quantization of $\eta(w)$. The soft threshold[35] can be defined as

$$\eta(w)=\begin{cases}(w-\mathrm{sgn}(w)t)I, & |w|>t,\\ 0, & |w|\leqslant t,\end{cases} \tag{13}$$

where sgn() is a sign function.

(8) Due to the aliasing of some useful high-frequency components in the mth order components, the mth order IMF component and all preceding components are subjected to wavelet thresholding denoising.

(9) The wavelet coefficients of each IMF component processed in (8) is reconstructed to obtain the first m components $IMF'(1)-IMF'(m)$ after noise elimination.

(10) The high-frequency components are reconstructed from $IMF'(1)$ to $IMF'(m)$. The low-frequency components are reconstructed from $IMF(m+1)$ to $IMF(n)$. And the denoised signal $x'(t)$ obtained by the trend term is

$$x'(t)=\sum_{i=1}^{m}c_i'(t)+\sum_{m+1}^{n}c_i(t)+r_n(t). \tag{14}$$

The above is the specific content of the joint algorithm model, and the overall process of the joint algorithm is shown in Fig.2.

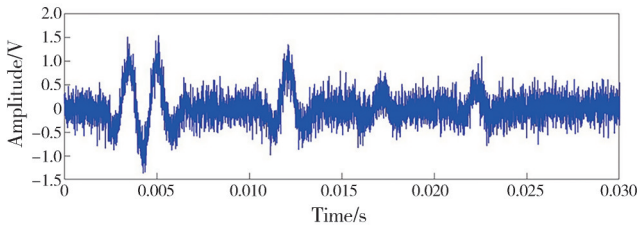

(a) Signal with noise

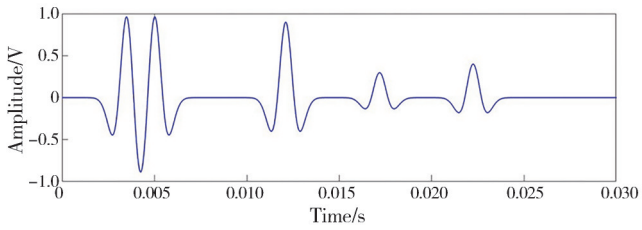

(b) Signal after denoising

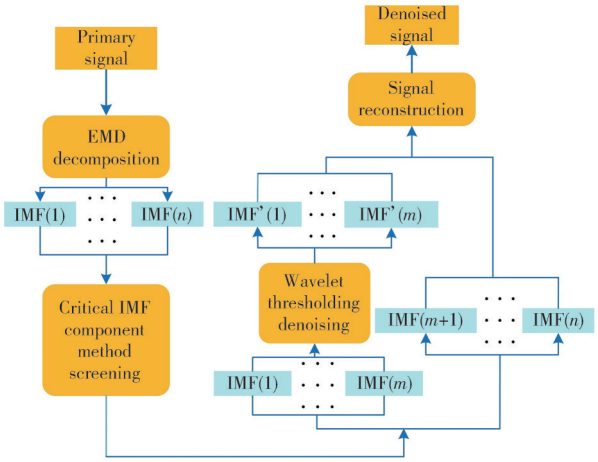

(c) Flowchart of joint noise cancellation algorithm

Fig. 2 Overall process of joint algorithm

2 Simulation design and analysis

2.1 Simulation signal

In detecting buried non-metallic pipelines, the acoustic signals generated by the seismic source propagate through the soil medium, including longitudinal and transverse waves (collectively referred to as body waves). Because the distance from the seismic source to the detector is less than the distance through the pipeline surface, the detector will receive both direct and reflected waves. Direct waves are the part of sound waves that directly reach the detector, while reflected waves are the part of sound waves that propagate back to the ground after being reflected at the contact surface between soil and pipelines. Therefore, the time-domain signal measured by the detector consists of direct and reflected waves. The mathematical expression is

$$s(t)=s_1(t)+s_2(t), \tag{15}$$

where s represents the output signal of the original detector; s_1 means the direct wave, and s_2 represents the reflected echo.

However, in addition to receiving various types of acoustic signals, detectors can also pick up a large amount of random noise interference from the internal and external environment of the detection instrument, most of which exhibit nonlinear and non-stationary characteristics. Therefore, the actual detector measurement signal should also include noise.

It has been stated that the short-time pulse excitation signal selected for the sound source is a Rayleigh wave, and the detector on the ground can detect multiple sound wave signals, such as direct waves and various types of reflected waves. Therefore, the sound wave signal received by the detector can be considered to be composed of a series of stacked Ricker wave components, and the mathematical expression of the actual measurement signal of the detector is

$$y(t)=\sum_{i=1}^{N}A_i(1-2(\pi f(t-t_0-t_i))^2)\mathrm{e}^{-(\pi f(t-t_0-t_i))^2}+n(t), \tag{16}$$

where N represents the number of pulses; A_i and t_i respectively represent the amplitude of the ith Ricker wavelet component and the offset from the starting time ($t=0$).

The original geophone measurement signal is simulated using a superposition of six sub-waves with a main frequency f of 500 Hz. These six sub-waves cover two direct waves (direct longitudinal waves and direct transverse waves) and four types of reflected waves (longitudinal-longitudinal waves, longitudinal-transverse waves, transverse-longitudinal waves, and transverse-transverse waves). The mathematical expression is

$$\begin{aligned}s(t)=&A_1(1-2(\pi f(t-t_0-t_1))^2)\mathrm{e}^{-(\pi f(t-t_0-t_1))^2}+\\&A_2(1-2(\pi f(t-t_0-t_2))^2)\mathrm{e}^{-(\pi f(t-t_0-t_2))^2}+\\&A_3(1-2(\pi f(t-t_0-t_3))^2)\mathrm{e}^{-(\pi f(t-t_0-t_3))^2}+\\&A_4(1-2(\pi f(t-t_0-t_4))^2)\mathrm{e}^{-(\pi f(t-t_0-t_4))^2}+\\&A_5(1-2(\pi f(t-t_0-t_5))^2)\mathrm{e}^{-(\pi f(t-t_0-t_5))^2}+\\&A_6(1-2(\pi f(t-t_0-t_6))^2)\mathrm{e}^{-(\pi f(t-t_0-t_6))^2},\end{aligned} \tag{17}$$

where the values of the individual parameters are $A_1=1$, $A_2=1$, $A_3=0.9$, $A_4=0.2$, $A_5=0.1$, $A_6=0.2$, $t_0=0.002$ s, $t_1=0.002\,5$ s, $t_2=0.005\,0$ s, $t_3=0.0104$ s, $t_4=0.015\,8$ s, $t_5=0.015\,4$ s, $t_6=0.020\,8$ s.

The original waveform of the obtained analogue signal is shown in Fig.3. Fig.4 shows the time-domain waveform of the noise-containing detector signal after adding Gaussian white noise with a signal-to-noise ratio of 1 dB.

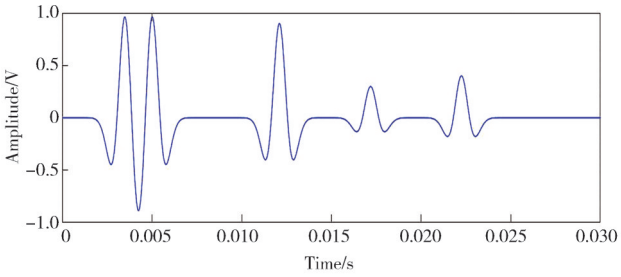

Fig. 3 Original geophone signal waveform

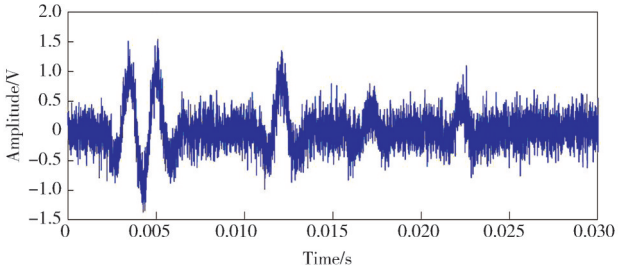

Fig. 4 Noise detector signal waveform

2.2 Criteria for judging filtering effect

The simplest way to judge whether the signal filtering effect is good or bad is to directly observe the filtered signal time-domain waveform and the original signal time-domain waveform proximity. The closer the two signal waveforms, the better the filtering effect is. However, when the difference between the waveforms is not apparent, the signal-to-noise ratio *SNR* and root-mean-square error *RMSE* can be used to judge. The higher *SNR* indicates that the proportion of valuable components in the signal after noise reduction is larger, and the root mean square error *RMSE* describes the average degree of deviation between the filtered signal and the original signal. Therefore, the larger the *SNR* and the lower the root mean square error *RMSE* of the signal after denoising, the better the filtering effect is represented. Assuming that $\hat{s}(t)$ is an approximate estimation of the original signal $s(t)$ extracted from the noised signal $y(t)$ by filtering, the expressions for the calculation of the input signal-to-noise ratio SNR_{in}, the output signal-to-noise ratio SNR_{out}, and the root-mean-square error *RMSE* are obtained by

$$SNR_{in}=10\lg\left(\frac{\sum_{k=1}^{N}s^2(k)}{\sum_{k=1}^{N}n^2(k)}\right), \tag{18}$$

$$SNR_{out}=10\lg\left(\frac{\sum_{k=1}^{N}s^2(k)}{\sum_{k=1}^{N}[s(k)-\hat{s}(k)]^2}\right), \tag{19}$$

$$RMSE=\sqrt{\frac{1}{N}\sum_{k=1}^{N}[s(k)-\hat{s}(k)]^2}, \tag{20}$$

where k is the time series, and N is the number of data points.

From the two mathematical expressions of SNR_{out} and *RMSE*, it can be seen that the smaller $\sum_{K=1}^{N}\left[s(k)-\hat{s}(k)\right]^2$ is, the larger the output SNR_{out}, and the smaller the root mean square error *RMSE* is, indicating the better denoising effect. Therefore, it can be considered that the decision rule is as follows. After doing the filtering process on the noise-containing signal $y(t)$, the *SNR* and *RMSE* of the denoised signal $\hat{s}(t)$ are solved, and if the *SNR* is bigger and the *RMSE* is smaller, it is considered that the denoising effect is better.

2.3 Comparative analysis of three denoising methods

2.3.1 Simulation results

The wavelet basis function suitable for denoising detector signals needs to simultaneously satisfy orthogonality, tight support, and approximate symmetry. According to Table 1, only the db wavelet, sym wavelet, coif wavelet, and haar wavelet meet the requirements. However, the continuity and smoothness of the Haar wavelet are relatively poor, so only the first three wavelets will be used for simulation experiments in the future, and the most suitable wavelet basis for denoising the detector signal will be found based on the simulation results.

Table 1 Functional properties of commonly used wavelet basis functions

Wavelet basis function	Orthogonality	Double orthogonality	Symmetry	Tight support	Continuous wavelet transform	Discrete wavelet transform
Haar (haar)	Have	Have	Symmetric	Have	Yes	Yes
Daubechies (db)	Have	Have	Approximate	Have	Yes	Yes
Biorthgonal (bior)	Not	Have	Asymmetric	Have	Yes	Yes
Coiflets (coif)	Have	Have	Approximate	Have	Yes	Yes
Symlets (sym)	Have	Have	Approximate	Have	Yes	Yes
Morlet (morl)	Not	Not	Symmetric	Not	Yes	No
Mexican hat (mexh)	Not	Not	Symmetric	Not	Yes	No
Meyer (meyr)	Have	Have	Symmetric	Not	Yes	Yes

MATLAB software was used to conduct simulation experiments. Firstly, it is necessary to identify the most suitable wavelet basis function for denoising detector data. Three types of wavelets, sym, db, and coif, are used to perform 5-layer wavelet decomposition on detector signals with input signal-to-noise ratios of 1 dB and 10 dB,

respectively.

The traditional wavelet threshold is

$$\lambda = \sigma\sqrt{2\lg N}, \tag{21}$$

where N is the length of the signal, and σ is the variance of the noise. Because in practical applications, the variance of the noise is generally unknown and usually needs to be estimated. The currently widely used threshold estimation methods include sqtwolog, rigrsure, heursure, and minimaxi.

In the simulation of selecting wavelet bases, the threshold estimation method is sqtwolog, and the decomposed wavelet coefficients are denoised by soft threshold function. Tables 2 and 3 show the output signal-to-noise ratios and root mean square error values of signals denoised using different wavelet bases under different input signal-to-noise ratio conditions.

Table 2 Denoising results of SNR_{in}=1 dB signal using db wavelet bases

db wavelet basis	SNR_{out}/dB	*RMSE*
1	12.621 3	0.057 97
2	16.304 9	0.037 93
3	16.361 9	0.037 69
4	16.080 5	0.042 36
5	16.273 2	0.038 93
6	16.440 3	0.037 35
7	16.034 6	0.039 13
8	16.049 9	0.039 06
9	16.386 4	0.037 6
10	16.175 3	0.038 5

Table 3 Denoising results of SNR_{in}=1 dB signal using sym wavelet bases

sym wavelet basis	SNR_{out}/dB	*RMSE*
1	12.621 3	0.057 97
2	16.304 9	0.037 93
3	16.361 9	0.037 69
4	16.261	0.038 13
5	16.476 9	0.037 19
6	16.23	0.038 26
7	16.036	0.039 13
8	16.164 2	0.038 55
9	16.416 1	0.037 45
10	16.084 6	0.038 91

Tables 2－7 show that at lower input signal-to-noise ratios, the denoising ability of the db wavelet and sym wavelet is better than that of the coif wavelet. The three wavelets corresponding to the best denoising ability are db6, sym5, and coif2 wavelet.

Table 4 Denoising results of SNR_{in}=1 dB signal using coif wavelet bases

coif wavelet basis	SNR_{out}/dB	*RMSE*
1	16.080 1	0.038 93
2	16.279 5	0.038 05
3	16.047 0	0.039 08
4	16.002 2	0.039 28
5	16.083 9	0.038 91

Table 5 Denoising results of SNR_{in}=10 dB signal using coif wavelet bases

coif wavelet basis	SNR_{out}/dB	*RMSE*
1	23.557 2	0.016 46
2	25.883 6	0.012 59
3	25.684 5	0.012 88
4	25.487 7	0.013 18
5	25.444 3	0.013 25

Table 6 Denoising results of SNR_{in}=10 dB signal using db wavelet bases

db wavelet basis	SNR_{out}/dB	*RMSE*
1	14.858 5	0.044 81
2	23.246 4	0.017 06
3	25.578 3	0.013 04
4	25.463 0	0.013 22
5	25.419 9	0.013 28
6	25.954 2	0.012 49
7	25.710 1	0.012 85
8	25.408 7	0.013 30
9	25.781 1	0.012 74
10	25.865 7	0.012 62

Table 7 Denoising results of SNR_{in}=10 dB signal using sym wavelet bases

sym wavelet basis	SNR_{out}/dB	*RMSE*
1	14.858 5	0.044 81
2	23.246 4	0.017 06
3	25.578 3	0.013 04
4	25.812 6	0.012 7
5	25.632 5	0.012 96
6	25.881 6	0.012 6
7	25.406 3	0.013 3
8	25.844 2	0.012 65
9	25.822 1	0.012 68
10	25.766 8	0.012 76

At higher input signal-to-noise ratios, the overall denoising ability of the sym wavelet is better than the other two wavelets, and the best denoising effects for each of the three wavelets are db6, sym6, and coif2 wavelets.

For noisy signals with a lower signal-to-noise ratio of SNR_{in}=3 dB, db6, sym5, and coif2 wavelets were used for denoising at different decomposition levels. For noisy signals with a higher signal-to-noise ratio of SNR_{in}=20 dB, db6, sym6, and coif2 wavelets are used for denoising at different decomposition levels. Fig.5(a) and 5(b) compare the output signal-to-noise ratio SNR_{out} of the signals after denoising with varying decomposition levels. When the number of decomposition layers exceeds 6, the signal-to-noise ratio begins to decrease.

Under soft threshold conditions, noisy signals with signal-to-noise ratios of －5 dB and 5 dB are denoised, and the db6 wavelet basis was selected based on the previous simulation analysis. 6-layer decomposition was chosen. Four different threshold estimation methods (rigrsure, heursure, aqtwolog, and minimaxi) were selected for simulation. The results are shown in Fig.6.

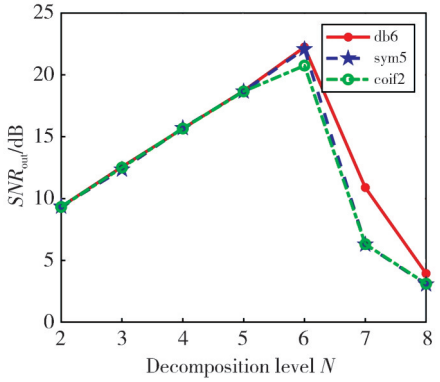

(a) SNR_{in}=3 dB

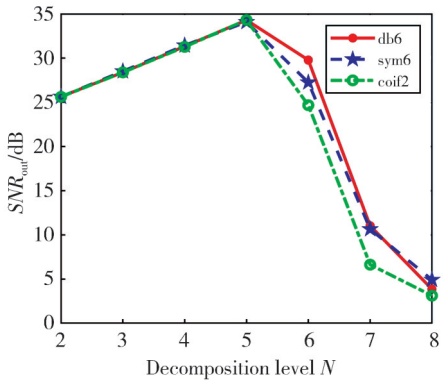

(b) SNR_{in}=20 dB

Fig. 5 Comparison of SNR_{out} after denoising with different decomposition levels

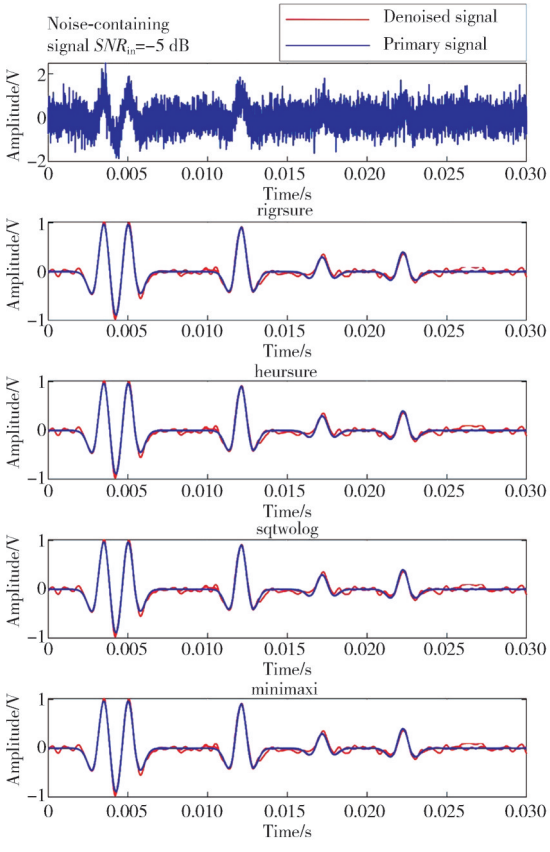

(a) Noise reduction results of four threshold estimation methods for signals with SNR_{in}=−5 dB

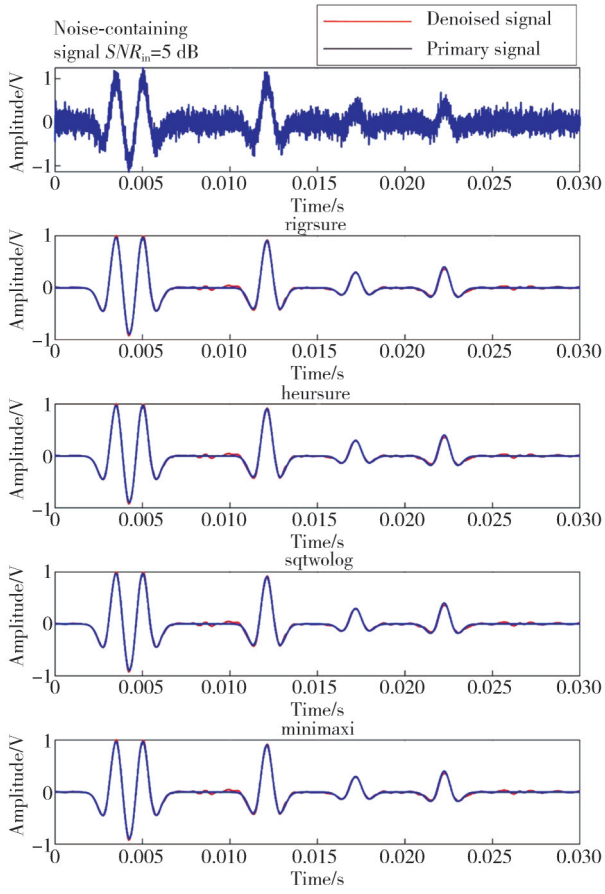

(b) Noise reduction results of four threshold estimation methods for signals with SNR_{in}=5 dB

Fig. 6 Denoising results of four threshold estimation methods

The denoising effect of the four thresholding methods on the detector measurement signal is similar, the signal waveform recovery after denoising is almost the same, and the output signal-to-noise ratio is also improved to the same extent. Therefore, a threshold calculation method is arbitrarily chosen for subsequent simulation studies.

Combining the conclusions drawn from the previous separate wavelet thresholding studies, db6 (6-layer decomposition) is used for all wavelet bases involved in the threshold noise reduction process, and the threshold estimation method and threshold function are selected as minimaxi and soft threshold, respectively. Figs. 7 — 12 compare the waveforms of signals with signal-to-noise ratios of — 5 dB and 5 dB with the original signal waveforms after noise reduction using the three noise reduction methods, respectively.

It can be seen that the denoised signals obtained by the three methods have a certain degree of distortion at the peak when SNR_{in}= — 5 dB and SNR_{in}=5 dB, and the resulting waveforms are still jittery.

However, the signal processed by the joint denoising method of wavelet thresholding and EMD is smoother,

the denoised signal has the best waveform match with the original signal, and the signal itself is less distorted. It can be seen that this method can weaken the energy loss of the useful signal while rejecting more noise.

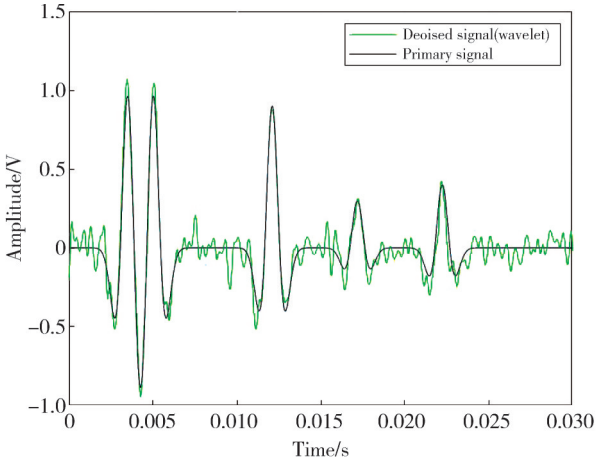

Fig. 7 Wavelet thresholding denoising result ($SNR_{in}=-5$ dB)

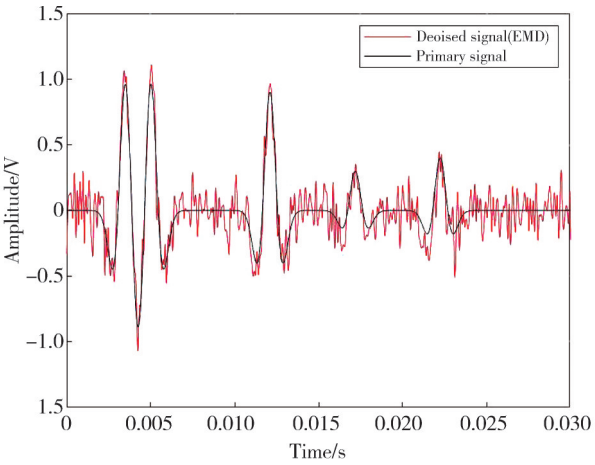

Fig. 8 EMD denoising result ($SNR_{in}=-5$ dB)

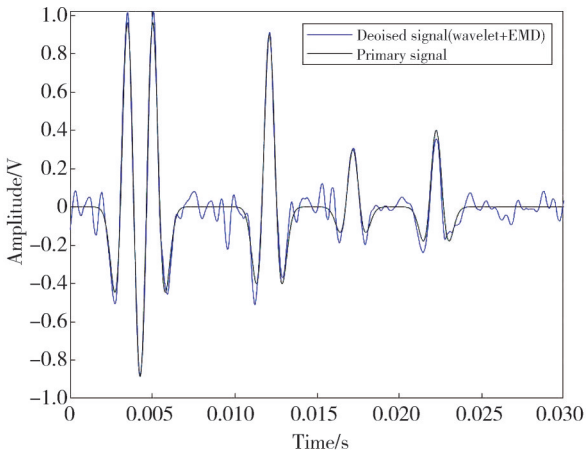

Fig. 9 Joint denoising result ($SNR_{in}=-5$ dB)

2.3.2 Evaluation of filtering effect of three denoising methods

Due to the weak reflection waves of the pipeline measured in this study, the input signal-to-noise ratio SNR_{in} was changed to -10 dB, -5 dB, 0 dB, 5 dB, and 10 dB for denoising analysis. The changes in the denoising effect comparison indicators under three different denoising methods and different noise environments are shown in Figs.13 and 14.

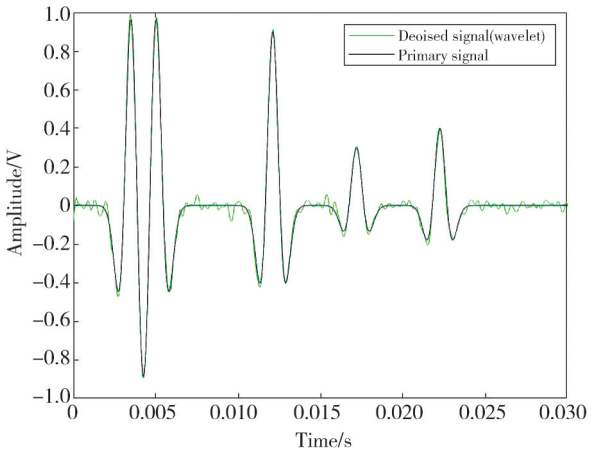

Fig. 10 Wavelet thresholding denoising result ($SNR_{in}=5$ dB)

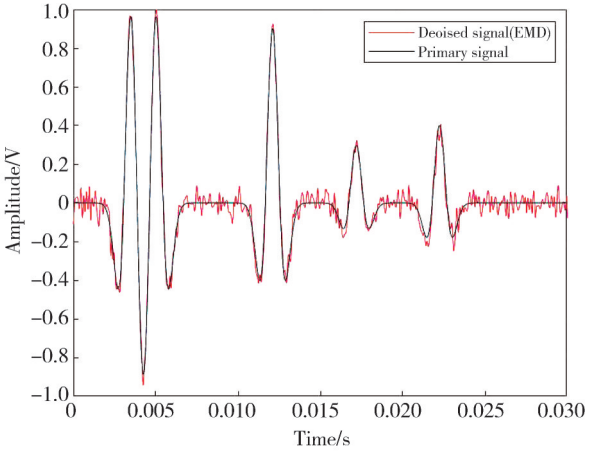

Fig. 11 EMD denoising result ($SNR_{in}=5$ dB)

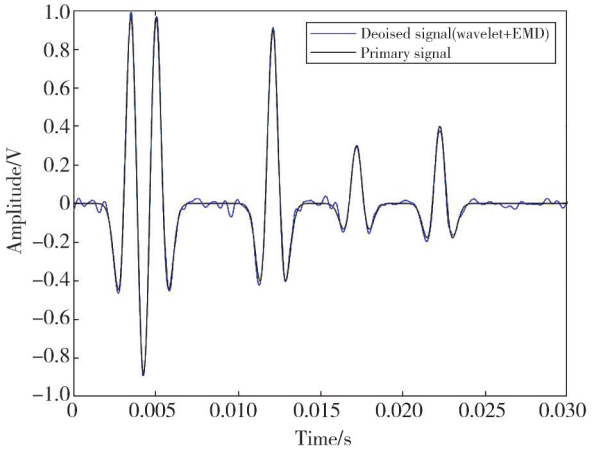

Fig. 12 Joint denoising result ($SNR_{in}=5$ dB)

Comparing the denoising results of echo signals with different noise levels, it is found that these methods consistently improve the quality of echo signals. Among them, the joint denoising method of wavelet threshold and EMD has the highest output signal-to-noise ratio SNR_{out} and the smallest root mean square error *RMSE*

under different input signal-to-noise ratios, followed by wavelet threshold method and EMD denoising method.

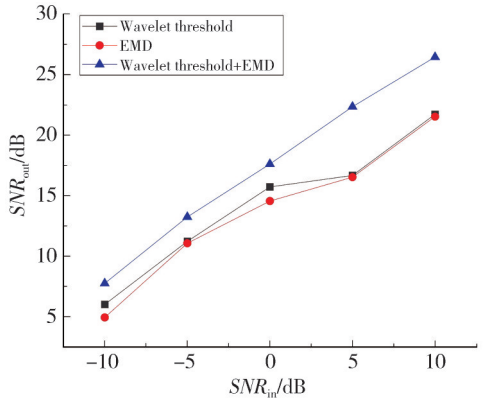

Fig. 13 SNR_{out} comparison chart

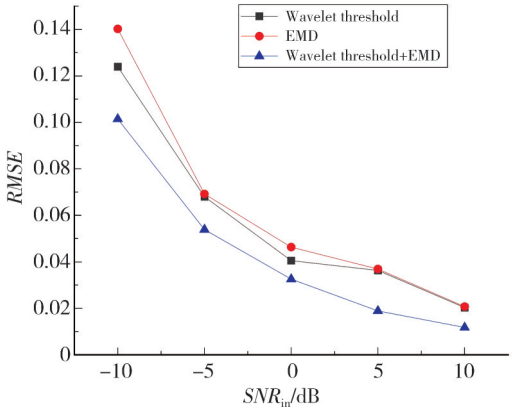

Fig. 14 *RMSE* comparison chart

From Tables 8 and 9, it can be seen that when the SNR_{in} is between −10 dB and 10 dB, the SNR_{out} of the joint denoising algorithm increases by 12%—34.1% compared to the wavelet threshold method and by 19.60%—56.8% compared to the EMD denoising method.

Table 8 Comparison of SNR_{out} of three methods at different input signal-to-noise ratios

SNR_{in}/dB	SNR_{out}/dB		
	Wavelet threshold	EMD	Wavelet threshold+EMD
−10	6.017 9	4.944 8	7.756 8
−5	11.227 7	11.076 4	13.249 1
0	15.731 3	14.562 9	17.619 3
5	16.674 6	16.539 0	22.355 9
10	21.728 1	21.541 6	26.461 4

Table 9 Comparison of RMSE of three methods at different input signal-to-noise ratios

SNR_{in}/dB	*RMSE*		
	Wavelet threshold	EMD	Wavelet threshold+EMD
−10	0.123 970	0.140 270	0.101 480
−5	0.068 048	0.069 244	0.053 920
0	0.040 517	0.046 351	0.032 601
5	0.036 348	0.036 919	0.018 898
10	0.020 314	0.020 755	0.011 780

Compared to wavelet thresholding methods, *RMSE* reduces by 18.1%—48%. And compared to EMD denoising methods, it reduces by 22.1%—48.8%. By comparing *SNR* and *RMS* error, it can be seen that although parameters such as wavelet basis are difficult to determine, only threshold processing of high-frequency components removed after EMD decomposition can effectively extract the effective information of high-frequency components, thus significantly improving the SNR of reconstructed signals and significantly reducing the RMS error.

When the signal-to-noise ratio is −5 dB and 5 dB, the denoising results of the detector are shown in Fig. 15(a) and (b). All three denoising methods have apparent effects on noise quantity and amplitude reduction. Still, the denoised signals obtained by the joint denoising method based on wavelet thresholding and EMD have smoother curves and more apparent waveform spike characteristics. It means that the denoising level of this method is better and can extract useful information from the detector signal more effectively. In a comprehensive view, the denoising level of the joint denoising algorithm of wavelet and EMD is better than that of the other two methods.

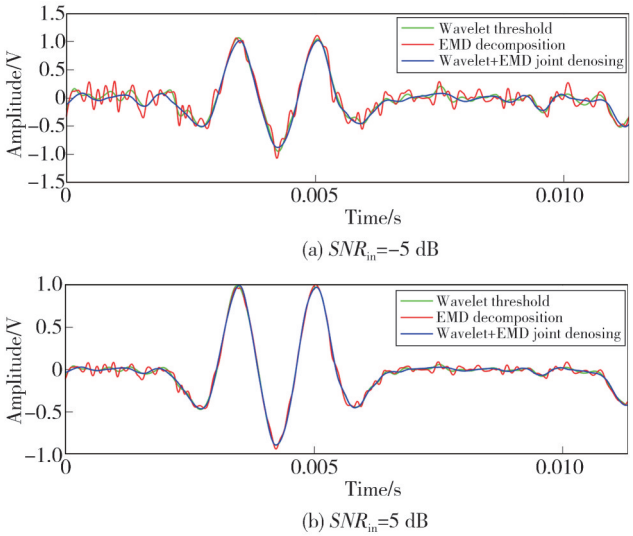

Fig. 15 Denoising results at different SNR_{in}

3 Experiment

3.1 Experimental platform construction

The acoustic detection system for buried non-metallic pipelines constructed in this article includes parts such as a seismic source, detector array, data acquisition module, power supply, DC transformer, and upper computer. According to the requirements of pipeline detection for excitation signal frequency and power, a

WD-12-inch active subwoofer horn with a frequency response range of 35 Hz—3 400 Hz, rated power of 600 W, and peak power of 1 200 W is selected as the sound source for the detection system. Select a Class D 8808.1 digital high-power amplifier with a frequency response range of 10 Hz—300 kHz and a maximum output power of 3 000 W to amplify the excitation signal. The power of the power supply determines the actual output power. Select an S-1200 W-12 V high-power DC transformer to convert the 220 V AC signal output by the mobile power supply into a 12 V DC signal for the power amplifier power supply, with a maximum output power of 1 200 W. Five highly sensitive LGT-VX1000 vibration amplifiers were selected as detectors to collect acoustic signals on the ground. The reference detector is placed next to the sound source and mainly used to correct the starting time of the detector signal.

3.2 Experiment and analysis

The previous chapter used simulation experiments to analyze the denoising effects of wavelet threshold denoising, EMD decomposition denoising, and a joint denoising method combining the two methods. Next, the denoising effects of these three methods were compared with actual detector data.

For 0.4 m and 1 m pipelines, a measuring line was arranged in each direction perpendicular to the pipeline direction. When the detector is 0.4 m away from the sound source, it is difficult to detect the sound wave signal.

The delay problem of the collected original detector data still exists, and it can be corrected based on the reference detector data. Figs.16 and 17 show the waveforms of each detector after time correction when the pipeline burial depth is 0.4 m and 1 m, respectively.

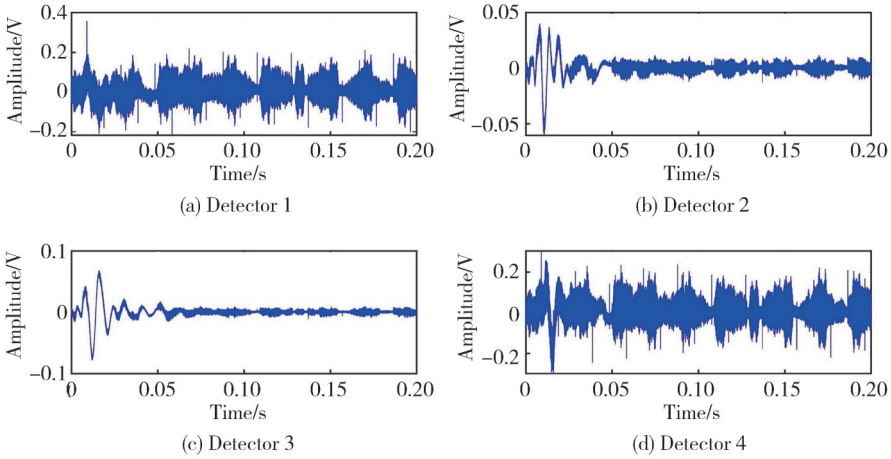

Fig. 16 Time-corrected geophone signal (pipe burial depth of 0. 4 m)

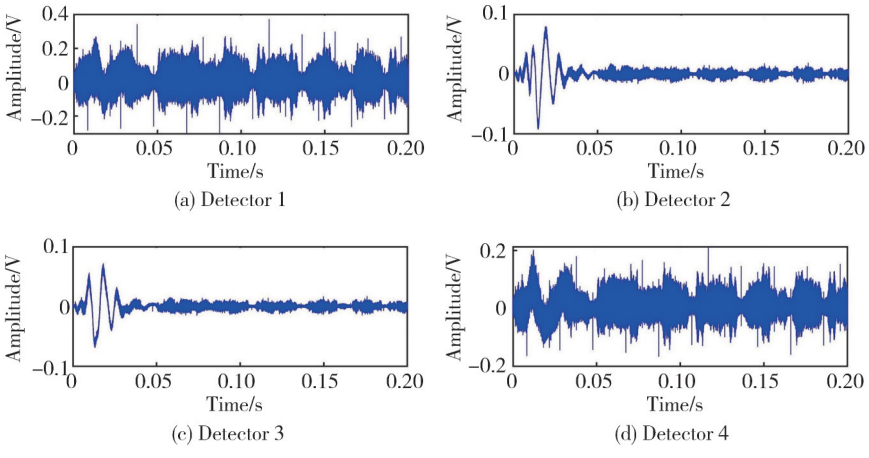

Fig. 17 Time-corrected geophone signal (pipe burial depth of 1 m)

Due to the proximity of detector 2 and detector 3 to the sound source, the sound wave signal is the main component, and the waveform is relatively clear. However, detectors 1 and 4 are further away from the sound source, and the greater the distance, the greater the attenuation, resulting in almost all useful sound wave signals being obscured by noise and challenging to observe. Therefore, it is necessary to denoise the detector data.

Due to the symmetrical arrangement of detector 1 and

detector 4, detector 2, and detector 3 concerning the sound source, the data from detector 1 and detector 3 in Fig. 17 are used as representatives, and three different denoising methods are applied to denoise them. The part related to wavelet threshold denoising uses db6 wavelet for 6-layer wavelet decomposition, and the threshold estimation method uses minimaxi. The threshold function is a soft threshold. The denoising results of detector 1 and detector 3 are shown in Figs.18 and 19.

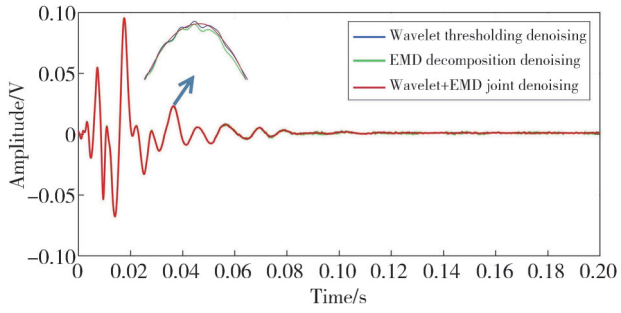

(a) Overall image of detector 1 waveform

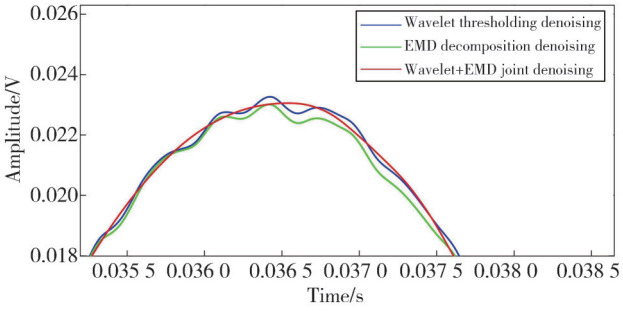

(b) Partial enlarged image of (a)

Fig. 18 Detector 1 waveform after signal denoising

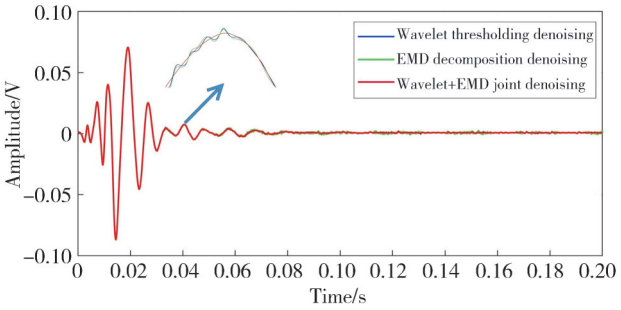

(a) Overall image of detector 3 waveform

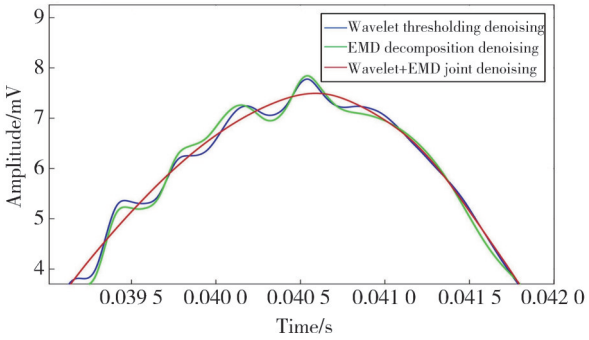

(b) Partial enlarged image of (a)

Fig. 19 Detector 3 waveform after signal denoising

The three denoising methods significantly reduce the quantity and amplitude of noise. By observing the enlarged local area, it can be seen that the denoising signal curve obtained by the joint denoising method based on wavelet threshold and EMD is smoother, and the waveform peak features are clearer. The red joint denoising waveform shows significant advantages.

Compared to other waveforms, the red waveform shows higher smoothness in the diagram, indicating that it is more effective in removing high-frequency noise. In addition, the peaks and feature points of the red waveform are clearer and more prominent, suggesting that it can effectively suppresses noise interference while retaining key information of the signal. In terms of the overall shape of the signal, the red waveform has a higher consistency with the ideal signal, which further confirms its excellent performance in denoising. Therefore, based on these observations, it can be concluded that the red waveform has significantly better denoising performance than other compared waveforms. This indicates that the joint method of wavelet thresholding and EMD has advantages in denoising levels and can more effectively extract useful information from detector signals, laying a good foundation for subsequent pipeline localization research.

4 Conclusions

This article studied the denoising technology for acoustic detection and positioning echo signals of buried non-metallic pipelines. Firstly, it analyzed the characteristics of interference signals mixed with useful echo signals. Secondly, a joint denoising algorithm combining EMD and wavelet thresholding was proposed to address the characteristics of the interference signals. Then, numerical simulation analysis was conducted on the denoising of useful echo signals, and the feasibility of the joint algorithm described in this article was verified. The study successfully overcame the issue of useful signal loss caused by traditional EMD algorithms when removing high-frequency noise, as well as the amplitude attenuation and signal loss problems in wavelet threshold denoising. By combining EMD decomposition with wavelet threshold denoising, the proposed method more effectively removed noise while maintaining the integrity of the signal. Experimental results showed that within the SNR range of −10 dB to 10 dB, the joint denoising algorithm significantly has improved the SNR and reduced the RMSE, demonstrating superior denoising performance compared to using EMD or wavelet thresholding methods alone. It provided a solid foundation

for the accurate positioning of pipeline locations.

However, the quality of signal transmission may be affected by external factors such as the position of the detectors, pipeline depth, and environmental noise and climate conditions. Future research will focus on reducing the impact of these factors on detection results and exploring denoising algorithms combined with machine learning to adapt to different pipelines and environmental conditions, ensuring the effectiveness and broad applicability of the methods.

Acknowledgement

This work was supported by Nanchong Southwest Petroleum University Science and Technology Strategic Cooperation Project (Nos. 23XNSYSX0022, 23XNSYSX0026); Provincial Science and Technology Plan Project (No. 2023ZHCG0020), and Southwest Petroleum University Natural Science "Sailing Plan" Project (No. 2023QHZ003).

Declaration of conflicting interests

The authors have no conflict of interests related to this publication.

References

[1] TAO X R, HE R Y, SHEN G T. Current status and development of in-use buried pipeline inspection technology. China Special Equipment Safety, 2005, 21: 41-45.

[2] LIANG L W. Experimental research on complex underground pipeline detection in urban districts. Xi'an: Northwest University, 2018.

[3] XU C. Research on buried non-metallic pipeline detection technology based on acoustic wave propagation characteristics. Anhui: Anhui University of Science and Technology, 2019.

[4] ZHAO H S. Research on the acoustic wave type underground pipe detector design. Shanghai: Shanghai University of Engineering Science, 2019.

[5] LI H M, FU Y R, ZHENG G J. Research on material suitability of Shenzhen metro water supply and drainage pipelines. Green Environmental Protection Building Materials, 2021(4): 25-26.

[6] LIU H, CHEN B, XIE M H, et al. Design of locator for buried non-metallic pipeline. Computer Measurement and Control, 2021, 29(5): 251-255.

[7] GE L, WANG T, FANG X, et al. Buried pipeline detection device and identification method based on capacitive tomography imaging. China Patent, 113945983A, 2022-01-18.

[8] MUGGLETON J M, RUSTIGHI E. Mapping the Underworld: recent developments in vibro-acoustic techniques to locate buried infrastructure. Géotechnique Letters, 2013, 3(3): 137-141.

[9] MUGGLETON J M, BRENNAN M J. The design and instrumentation of an experimental rig to investigate acoustic methods for the detection and location of underground piping systems. Applied Acoustics, 2008, 69(11): 1101-1107.

[10] MUGGLETON J M, BRENNAN M J, GAO Y. Determining the location of buried plastic water pipes from measurements of ground surface vibration. Journal of Applied Geophysics, 2011, 75(1): 54-61.

[11] ZHANG Y H, L S, WANG J Q. On the similarities and differences between the positioning of acoustic positioning instruments and the positioning of detectable warning strips for gas buried PE pipelines. Consumer Electronics Magazine, 2021(9): 53-55.

[12] GAO Y, CUI X W. A device and method for detecting buried pipelines using acoustic reflection. China Patent, 201810083685.9, 2019-07-09.

[13] GE L, HE J, GAO Y, et al. Localisation of buried PE pipes by acoustic imaging method using time-domain superposition. Acta Acustica, 2024, 49(3): 569-576.

[14] GONG Y, JIA R S, LU X M, et al. Suppression of random noise in microseismic signals using empirical modal decomposition and wavelet transform. Journal of China Coal Society, 2018, 43(11): 3247-3256.

[15] GE W Q, ZHANG K, LIU C Z. Signal preprocessing of gas ultrasonic flowmeter based on wavelet threshold algorithm. Acta Metrologica Sinica, 2024, 45(10): 1502-1511.

[16] ARTINA M, FORNASIER M, SOLOMBRINO F. Linearly constrained nonsmooth and nonconvex minimization. SIAM Journal on Optimization, 2013, 23(3): 1904-1937.

[17] HUI T, ZHAO G C, SU J, et al. Improved empirical modal decomposition for noise reduction of atomic clock data. Journal of Henan University of Science & Technology (Natural Science), 2021, 42(5): 45-50.

[18] WANG T. Research on EMD algorithm and its application in signal denoising. Harbin: Harbin Engineering University, 2010.

[19] SHI Z Y, XU W M, ZHOU B, et al. Adaptive noise reduction method based on empirical modal decomposition and wavelet thresholding. Hydrographic Surveying and Charting, 2021, 41(6): 54-57.

[20] FEI H L, LIU M, QU G J, et al. Noise reduction method for blast vibration signal based on ensemble empirical modal decomposition-wavelet thresholding method. Explosion and Shock Waves, 2018, 38(1): 112-148.

[21] GUO F, WANG P. Joint denoising algorithm for MEMS vector hydrophones based on ensemble empirical mode decomposition. Journal of Test and Measurement Technology, 2022, 36(2): 117-121.

[22] SHAO R P, HU W T, LI J. Multi-fault feature extraction and diagnosis of gear transmission system using time-

frequency analysis and wavelet threshold de-noising based on EMD. Shock and Vibration, 2013, 20(4): 763-780.
[23] LU Q, PANG L X, HUANG H Q, et al. High-G calibration denoising method for high-G MEMS accelerometer based on EMD and wavelet threshold. Micromachines, 2019, 10(2): 134.
[24] DING H B. Research on comparative analysis of denoising methods for LiDAR signals. Hefei: University of Science and Technology of China, 2022.
[25] XU F H, WANG Z W, LIU J H, et al. Application of de-noising method on electrical imaging logging data based on joint EMD and wavelet threshold. Journal of China University of Petroleum, 2020, 44(3): 56-65.
[26] ZHANG Y Y, YANG Z X, DU X L, et al. A new method for denoising underwater acoustic signals based on EEMD, correlation coefficient, permutation entropy, and wavelet threshold denoising. Journal of Marine Science and Application, 2024, 23(1): 222-237.
[27] LI L Z, PAN C R, REN Y K, et al. Application of EMD and wavelet thresholding combined denoising method on magnetic induction sorter. Nonferrous Metals (Mineral Processing Section), 2023(6): 140-148.
[28] SUN G, ZHANG R, LIU Z, et al. EMD-based noise reduction study of steel cored conveyor belt containing slag signal. Alexandria Engineering Journal, 2024, 98: 56-67.
[29] GE L, HE J, GAO Y, et al. Localisation of buried PE pipes by acoustic imaging method using time-domain superposition. Acta Acustica, 2024, 49(3): 569-576.
[30] GE L, WANG T, XIAO X T, et al. A new acoustic positioning method for buried PE pipeline based on time-domain superposition. Natural Gas Industry, 2022, 42(9): 111-121.
[31] PAPANDREOU B, RUSTIGHI E, BRENNAN M J. On the detection of objects buried at a shallow depth using seismic wave reflections. The Journal of the Acoustical Society of America, 2011, 129(3): 1366-1374.
[32] XU L L, ZHANG J, ZHAO G Y. Design method of nonlinear scanning signal for controllable seismic source based on damped Rayleigh waves. Oil Geophysical Prospecting, 2022, 57(3): 540-549.
[33] YANG R H. Analysis of the influence of inverse time migration source wavelet. Progress in Geophysics, 2021, 36(5): 2102-2108.
[34] ZHANG X, WANG H L. Static boosted wavelet denoising method based on optimal decomposition scale. High Voltage Engineering, 2009, 35(3): 501-508.
[35] XIE H J, LI J R, DONG Y, et al. Influence of wavelet base and threshold parameters on denoising effect of transient electromagnetic signals. Journal of Xi'an University of Science and Technology, 2020, 40(4): 682-690.

基于EMD与小波阈值联合去噪的埋地非金属管道声学定位回波信号提取

葛　亮[1*], 袁雪峰[1], 肖小汀[2], 骆　平[3], 王　甜[1]

1. 西南石油大学 机电工程学院, 四川 成都 610500;
2. 西南石油大学 电气信息学院, 四川 成都 610500;
3. 中国移动(成都)产业研究院, 四川 成都 610200

摘　要: 在埋地非金属管道的声学探测过程中, 回波信号往往受到大量噪声的干扰, 这使得有效提取有用信号变得极为困难。本文提出了一种结合经验模态分解(EMD)与小波阈值去噪的算法, 该方法充分考虑了回波信号的非线性和非平稳性特征, 使得去噪效果更为显著。通过数值仿真, 验证了该方法的可行性和有效性。从数值结果上看, 当SNR_{in}在−10 dB与10 dB之间时, 联合去噪算法的SNR_{out}在小波阈值方法的基础上增加了12.0%—34.1%, 在EMD去噪方法的基础上增加了19.6%—56.8%; 联合去噪算法的*RMSE*在小波阈值方法基础上降低了18.1%—48.0%, 在EMD去噪方法的基础上降低了22.1%—48.8%。实验结果表明, 这种联合的去噪算法不仅能有效减少噪声干扰, 还能显著提高声学探测的定位精度。研究成果可为埋地非金属管道的回波信号去噪提供技术支撑, 有利于提高声学对地下非金属管道的探测定位精度。

关键词: 埋地非金属管道; 声学定位; 信号处理; 最佳分解尺度; 小波基函数; EMD联合小波阈值算法

引用格式: GE Liang, YUAN Xuefeng, XIAO Xiaoting, et al. Acoustic location echo signal extraction of buried non-metallic pipelines based on EMD and wavelet threshold joint denoising. Journal of Measurement Science and Instrumentation, 2024, 15(4): 417-431.